Quasi-Spherical Approximation for Rotating Black Holes

Hisa-aki Shinkai† and Sean A. Hayward †,‡
shinkai@gravity.phys.psu.edu, hayward@mail.apctp.org
† *Centre for Gravitational Physics and Geometry, 104 Davey Laboratory,*
The Pennsylvania State University, University Park, PA 16802-6300, U.S.A.
‡ *Present address: Asia Pacific Center for Theoretical Physics,*
The Korea Foundation for Advanced Study Building 7th Floor, Yoksam-dong 678-39, Kangnam-gu, Seoul 135-081, Korea
(March 7, 2001 (revised version))

We numerically implement a quasi-spherical approximation scheme for computing gravitational waveforms for coalescing black holes, testing it against angular momentum by applying it to Kerr black holes. As error measures, we take the conformal strain and specific energy due to spurious gravitational radiation. The strain is found to be monotonic rather than wavelike. The specific energy is found to be at least an order of magnitude smaller than the 1% level expected from typical black-hole collisions, for angular momentum up to at least 70% of the maximum, for an initial surface as close as $r = 3m$.

PACS numbers: 04.25.-g, 04.25.Dm, 04.70.Bw, 04.20.Ha, 04.30.-w
Preprint numbers: gr-qc/0008075, CGPG-00/8-1

I. INTRODUCTION

A quasi-spherical approximation scheme in a 2+2 decomposition of the space-time has recently been introduced [1]. This proposal is with the aim of providing a computationally inexpensive estimate of the gravitational waveforms produced by a black-hole or neutron-star collision, given a full numerical simulation up to (or close to) coalescence, or an analytical model thereof.

The scheme truncates the Einstein equations by removing second-order terms which would vanish in a spherically symmetric space-time, cf. Bishop *et al.* [2]. Thus when the linearized fields vanish, spherical symmetry is recovered in full. Unlike previous work on null-temporal formulations [2,3], a dual-null formulation is adopted here, i.e. a decomposition of the space-time by two intersecting foliations of null hypersurfaces. Technical advantages of the scheme include that only ordinary differential equations need be solved, and that the dual-null formulation is adapted to radiation extraction. Advantages of applicability include that no prescribed background is required and that arbitrarily rapid dynamical processes (close to spherical symmetry) are allowed. The pressing question concerns how well the scheme handles deviations from spherical symmetry. The principal such deviation in the context of coalescing black holes is expected to be due to angular momentum. The primary test case is therefore Kerr black holes, the unique stationary vacuum black holes.

This article reports a numerical implementation of the quasi-spherical approximation and its application to Kerr black holes, taking Boyer-Lindquist quasi-spheres. Since Kerr spacetime is stationary and contains no gravitational radiation, what we will evaluate in this article is the spurious gravitational radiation produced by the approximation. The situation is quite different from adding perturbations [4] or strong waves [5] around the black hole as in other studies. We consider two measures of the error introduced by the approximation. Firstly, the practical measure is the waveform of the spurious strain, as compared to signals expected to be measured by interferometers. Secondly, we measure the specific energy, i.e. the ratio of the radiated energy E to the original mass m; this is a conservative measure, as it involves summing the errors over all angles of the sphere, whereas observation is restricted to a particular angle.

In principle these quantities depend on only the spin parameter a/m, the relative initial radius r_0/m and, in the case of the strain, the angle. For the approximation to be useful, the error should be significantly less than the values expected for a realistic black-hole collision. Typical values for the specific energy obtained from numerical simulations [6] or from the close-limit approximation [7] have increased from early estimates to around 1% if the initial relative momentum [8] or angular momentum [9] is appreciable. The theoretical limit on how badly an approximation might perform is much higher: 29% of the mass of a maximally rotating Kerr black hole may be extracted by the Penrose process [10].

The article is organized as follows. Section II describes the dual-null formalism, the quasi-spherical approximation and the observables, strain and energy. Section III describes our model and numerical integration procedures. The numerical results are shown in Section IV and we summarize the article in Section V.

II. FORMULATION AND APPROXIMATION

A. Dual-null formulation

The quasi-spherical approximation [1] is based on a dual-null formulation [11] of Einstein gravity [12], summarized as follows. One takes two intersecting families of null hypersurfaces labelled by $x^{\pm}$. Then the normal 1-forms $n^{\pm} = -dx^{\pm}$ satisfy

$$g^{-1}(n^{\pm}, n^{\pm}) = 0 \tag{2.1}$$

where g is the space-time metric. The relative normalization of the null normals may be encoded in a function f defined by

$$e^f = -g^{-1}(n^+, n^-). \tag{2.2}$$

Then the induced metric on the transverse surfaces, the spatial surfaces of intersection, is found to be

$$h = g + 2e^{-f} n^+ \otimes n^-, \tag{2.3}$$

where $\otimes$ denotes the symmetric tensor product. The covariant derivative of h is denoted by D. The dynamics is described by Lie transport along two commuting evolution vectors $u_{\pm}$:

$$[u_+, u_-] = 0. \tag{2.4}$$

Specifically, the evolution derivatives, to be discretized in a numerical code, are

$$\Delta_{\pm} = \perp L_{u_{\pm}}, \tag{2.5}$$

where $\perp$ indicates projection by h and L denotes the Lie derivative. There are two shift vectors

$$s_{\pm} = \perp u_{\pm}. \tag{2.6}$$

In a coordinate basis $(u_+, u_-; e_i)$ such that $u_{\pm} = \partial/\partial x^{\pm}$, where $e_i = \partial/\partial x^i$ is a basis for the transverse surfaces, the metric takes the form

$$\begin{aligned} g = h_{ij}(dx^i + s_+^i dx^+ + s_-^i dx^-) \otimes \\ (dx^j + s_+^j dx^+ + s_-^j dx^-) - 2e^{-f} dx^+ \otimes dx^-. \end{aligned} \tag{2.7}$$

Then $(h, f, s_{\pm})$ are configuration fields and the independent momentum fields are found to be linear combinations of

$$\theta_{\pm} = *L_{\pm} *1, \tag{2.8}$$
$$\sigma_{\pm} = \perp L_{\pm} h - \theta_{\pm} h, \tag{2.9}$$
$$\nu_{\pm} = L_{\pm} f, \tag{2.10}$$
$$\omega = \tfrac{1}{2} e^f h([l_-, l_+]), \tag{2.11}$$

where $*$ is the Hodge operator of h and $L_{\pm}$ is shorthand for the Lie derivative along the null normal vectors

$$l_{\pm} = u_{\pm} - s_{\pm} = e^{-f} g^{-1}(n^{\mp}). \tag{2.12}$$

Then the functions $\theta_{\pm}$ are the expansions, the traceless bilinear forms $\sigma_{\pm}$ are the shears, the 1-form ω is the twist, measuring the lack of integrability of the normal space, and the functions $\nu_{\pm}$ are the inaffinities, measuring the failure of the null normals to be affine. The fields $(\theta_{\pm}, \sigma_{\pm}, \nu_{\pm}, \omega)$ encode the extrinsic curvature of the dual-null foliation. These extrinsic fields are unique up to duality $\pm \mapsto \mp$ and diffeomorphisms which relabel the null hypersurfaces, i.e. $dx^{\pm} \mapsto e^{\lambda_{\pm}} dx^{\pm}$ for functions $\lambda_{\pm}(x^{\pm})$.

It is also useful to decompose h into a conformal factor Ω and a conformal metric k by

$$h = \Omega^{-2} k, \tag{2.13}$$

such that

$$\Delta_{\pm} \hat{*} 1 = 0, \tag{2.14}$$

where $\hat{*}$ is the Hodge operator of k, satisfying $*1 = \hat{*}\Omega^{-2}$. Taking quasi-spherical coordinates $x^i = (\theta, \phi)$ such that $\hat{*}1 = \sin\theta d\theta \wedge d\phi$, Ω^{-1} is the quasi-spherical radius. In an asymptotically flat space-time, it becomes convenient to use the conformally rescaled expansions and shears

$$\vartheta_{\pm} = \Omega^{-1} \theta_{\pm}, \tag{2.15}$$
$$\varsigma_{\pm} = \Omega \sigma_{\pm}, \tag{2.16}$$

since they are finite and generally non-zero at null infinity $\Im^{\mp}$.

B. Quasi-spherical approximation

Of the dynamical fields and operators introduced above, $(s_{\pm}, \sigma_{\pm}, \omega, D)$ vanish in spherical symmetry, while $(h, f, \theta_{\pm}, \nu_{\pm}, \Delta_{\pm})$ generally do not. The quasi-spherical approximation consists of linearizing in $(s_{\pm}, \sigma_{\pm}, \omega, D)$, i.e. setting to zero any second-order terms in these quantities. This yields a greatly simplified truncation [1] of the full field equations, the first-order dual-null form of the vacuum Einstein system [12]. In particular, the truncated equations decouple into a three-level hierarchy, the last level being irrelevant to determining the gravitational waveforms. The remaining equations are the quasi-spherical equations

$$\Delta_{\pm} \Omega = -\tfrac{1}{2} \Omega^2 \vartheta_{\pm}, \tag{2.17}$$
$$\Delta_{\pm} f = \nu_{\pm}, \tag{2.18}$$
$$\Delta_{\pm} \vartheta_{\pm} = -\nu_{\pm} \vartheta_{\pm}, \tag{2.19}$$
$$\Delta_{\pm} \vartheta_{\mp} = -\Omega(\tfrac{1}{2} \vartheta_+ \vartheta_- + e^{-f}), \tag{2.20}$$
$$\Delta_{\pm} \nu_{\mp} = -\Omega^2(\tfrac{1}{2} \vartheta_+ \vartheta_- + e^{-f}), \tag{2.21}$$

and the linearized equations

$$\Delta_{\pm} k = \Omega \varsigma_{\pm}, \tag{2.22}$$
$$\Delta_{\pm} \varsigma_{\mp} = \Omega(\varsigma_+ \cdot k^{-1} \cdot \varsigma_- - \tfrac{1}{2} \vartheta_{\mp} \varsigma_{\pm}). \tag{2.23}$$

These are all ordinary differential equations; no transverse D derivatives occur. Thus we have an effectively two-dimensional system to be integrated independently at each angle of the sphere.

The initial-data formulation is based on a spatial surface S orthogonal to $l_{\pm}$ and the null hypersurfaces $\Sigma_{\pm}$

generated from S by $l_\pm$, assumed future-pointing. The initial data for the above equations are $(\Omega, f, k, \vartheta_\pm)$ on S and $(\varsigma_\pm, \nu_\pm)$ on $\Sigma_\pm$. We will take l_+ and l_- to be outgoing and ingoing respectively.

C. Strain

The variables are directly related to physically measurable quantities. In particular,

$$\epsilon = \frac{1}{2}\int_\gamma \dot{k} d\tau \tag{2.24}$$

is the transverse strain tensor measured along a worldline γ normal to the transverse surfaces, where $\dot{k} = \bot L_\lambda k$ in terms of a vector $\lambda = \partial/\partial\tau$ tangent to γ. For a detector at large distance, one may apply the linearized approximation, where 2ϵ reduces to the transverse traceless metric perturbation of a linearized plane gravitational wave. In a weak gravitational field, one may use Newtonian physics, where ϵ reduces to the Newtonian strain tensor. Thus the displacements to be measured by an interferometer are

$$\frac{\delta\ell}{\ell} = \epsilon(e, e) \tag{2.25}$$

where the unit vector e is the direction of displacement.

Writing $\lambda = a^+ l_+ + a^- l_-$ yields

$$\epsilon = \frac{1}{2}\int_\gamma \Omega(a^+\varsigma_+ + a^-\varsigma_-)d\tau. \tag{2.26}$$

Since the strain vanishes at future null infinity $\Im^+$, it is convenient to use the conformal strain tensor

$$\varepsilon = \frac{1}{2}\int \varsigma_- dx^-, \tag{2.27}$$

where the integal is at constant x^+. We will denote its plus and cross components by $\varepsilon_+ = \varepsilon_{\theta\theta}$ and $\varepsilon_\times = \varepsilon_{\theta\phi}$. In order to compare with observational results, one converts back to the strain,

$$\epsilon = \frac{\varepsilon}{R}, \tag{2.28}$$

where R is the distance between the source and the detector.

D. Energy

We define the energy flux ϕ of the gravitational waves, or more conveniently, the conformal energy flux $\varphi = \Omega^{-2}\phi$, as the 1-form $\varphi = \varphi_+ dx^+ + \varphi_- dx^-$, where

$$\varphi_\pm = -\frac{e^f \vartheta_\mp k^{ab}k^{cd}\varsigma_{\pm ac}\varsigma_{\pm bd}}{64\pi}. \tag{2.29}$$

These expressions have the same form as those for the conformal Bondi flux at $\Im^\mp$ [1], but we propose using them locally. Then ϕ_- is the outgoing flux and ϕ_+ is the ingoing flux. The corresponding energy E of the gravitational waves is then given by

$$\Delta_\pm E = \oint \hat{*}\varphi_\pm \tag{2.30}$$

with the initial condition $E|_S = 0$. Thus the Bondi energy at $\Im^+$ is $E + E_0$, where E_0 is the Bondi energy at the intersection with Σ_+, which in the Kerr case will be just the ADM mass m. We propose using the specific energy E/m at $\Im^+$ as a measure of the strength of a black-hole collision, following various references [6–9]. This is the fraction of the original mass-energy which has radiated away.

III. MODEL AND NUMERICAL PROCEDURES

A. Model: Kerr black hole

As our model, we take a Kerr black-hole geometry,

$$\begin{aligned} ds^2 = &-\frac{\Delta}{\Sigma}[dt - a\sin^2\theta d\phi]^2 + \frac{\sin^2\theta}{\Sigma}[(r^2+a^2)d\phi - adt]^2 \\ &+\frac{\Sigma}{\Delta}dr^2 + \Sigma d\theta^2, \end{aligned} \tag{3.1}$$

where

$$\Delta = r^2 - 2mr + a^2 \tag{3.2}$$
$$\Sigma = r^2 + a^2\cos^2\theta \tag{3.3}$$

and m is the mass and am the angular momentum. The horizon radius is denoted by $r_H = m + \sqrt{m^2 - a^2}$. We take the quasi-spherical approximation adapted to these (Boyer-Lindquist) coordinates, i.e. the initial surface S is of constant $r = r_0$ and constant t, as depicted in Fig.1. The inaccuracy of the quasi-spherical approximation as measured by E/m then depends in principle only on a/m and r_0/m. We expect E/m to be monotonically increasing in a/m, from zero at $a = 0$ to a maximum at $a = m$, since angular momentum is the cause of the asphericity. Similarly, E/m is expected to be monotonically decreasing in r_0/m, to zero at infinity, since the approximation should be better at large distances.

B. Initial data

An explicit dual-null form of the Kerr metric is not known except on the symmetry axis [13] or in the Schwarzschild case, as the Kruskal form. Although there is an effort for this direction [14], we did not find explicit double-null coordinates which are well behaved at the outer horizons and infinity, despite trying changes

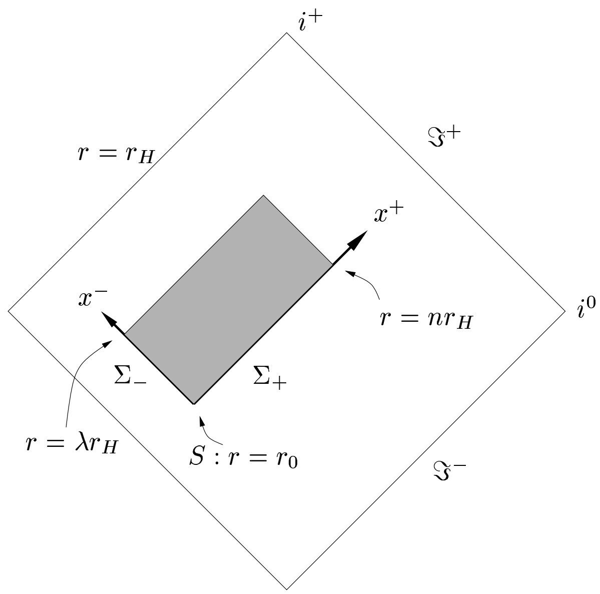

FIG. 1. The region of numerical integration is shown as the shaded region in the picture. Initial data is prescribed on a spatial surface S of constant Boyer-Lindquist $r = r_0$ and t, and the null hypersurfaces $\Sigma_\pm$ generated from it. On Σ_- (Σ_+), the x^- (x^+) coordinate is set so as to cover the region $\lambda r_H \le r \le r_0$ ($r_0 \le r \le nr_H$), where $1 < \lambda \approx 1$ and $n \gg 1$ are constants to be set by hand.

in angular coordinate and Kruskal-type rescalings [15]. However, we can construct the initial data analytically as functions of (r, θ), then convert to the required functions of $(x^\pm, \theta)$, as follows. We remark that our initial surfaces are $\Sigma_\pm$, and the following method applies outside the horizons.

The null normal vectors are initially given by

$$l_\pm|_{\Sigma_\pm} = \left(\frac{\Sigma}{2(\Delta - a^2\sin^2\theta)}\right)^{1/2} \partial_t \pm \left(\frac{\Delta}{2\Sigma}\right)^{1/2} \partial_r \quad (3.4)$$

where the normalization is such that

$$f|_S = 0. \quad (3.5)$$

The apparent degeneracy at $\Delta = a^2\sin^2\theta$ is just the boundary of the ergoregion where ∂_t becomes spatial; the dual-null coordinates extend through. We also fix

$$\nu_\pm|_{\Sigma_\pm} = 0, \quad (3.6)$$

which means that $x^\pm|_{\Sigma_\pm}$ are affine parameters. This implies $f|_{\Sigma_\pm} = 0$, fixing $l_\mp|_{\Sigma_\pm}$ and therefore locally determining the dual-null foliation.

The quasi-spherical conformal factor is

$$\Omega = \left((r^2+a^2)^2 - \Delta a^2 \sin^2\theta\right)^{-1/4} \quad (3.7)$$

which is real and positive. Then we obtain the conformal metric

$$k = \Omega^2\Sigma d\theta^2 + \frac{\sin^2\theta}{\Omega^2\Sigma} d\phi^2, \quad (3.8)$$

and the conformally rescaled expansions and shears

$$\vartheta_\pm|_S = \pm\sqrt{\frac{\Delta}{2\Sigma}}\Omega^3 U, \quad (3.9)$$

$$\varsigma_\pm|_{\Sigma_\pm} = \pm\sqrt{\frac{\Delta}{2\Sigma}}\Omega^5 V a^2 \sin^2\theta \left(d\theta^2 - \frac{\sin^2\theta}{\Omega^4\Sigma^2}d\phi^2\right), \quad (3.10)$$

where

$$U = -2\Omega^{-5}\partial_r\Omega = 2r(r^2+a^2) - (r-m)a^2\sin^2\theta, \quad (3.11)$$

$$V = \frac{\Omega^{-6}\partial_r(\Omega^2\Sigma)}{a^2\sin^2\theta} = r^3 + 3mr^2 + a^2(r-m)\cos^2\theta. \quad (3.12)$$

To complete the initial data construction, we need to know the initial data on $\Sigma_\pm$ as functions of $(x^\pm, \theta)$. So we need to know $r|_{\Sigma_\pm}$ as functions of $(x^\pm, \theta)$. This is determined by the equations

$$\Delta_\pm r|_{\Sigma_\pm} = \pm\left(\frac{\Delta}{2\Sigma}\right)^{1/2}, \quad (3.13)$$

giving

$$x_\pm|_{\Sigma_\pm} = \pm\int_{r_0}^{r}\left(\frac{2\Sigma}{\Delta}\right)^{1/2} dr', \quad (3.14)$$

where the integral is along a curve of constant (θ, ϕ). Note that the Δ factor means that we take S outside the horizons $r = r_H$, which anyway is the region of interest. We numerically integrated (3.14) using a fourth order Runge-Kutta method (Fehlberg method), then inverted. This was checked against the analytic solution in the equatorial plane $\theta = \pi/2$:

$$x^\pm|_{\Sigma_\pm} = \pm\sqrt{2}\left(\sqrt{\Delta} + m\ln(r - m + \sqrt{\Delta})\right) \mp c. \quad (3.15)$$

As m is an overall scale, we fixed it to unity.

C. Evolution procedures

Here we describe our numerical procedures. We have a set of ordinary differential equations in two variables. As pointed out by Gundlach and Pullin [16], free evolution schemes in such a system may lead to unstable evolution. This fact was also seen in our experience, and we developed a kind of predictor-corrector scheme similar to that of Hamadé and Stewart [17].

The actual steps we took are the followings. The set of variables is $u \equiv (\Omega, f, \vartheta_\pm, \nu_\pm, k_{ab}, \varsigma_{\pm ab})$. Let us schematically express a set u at a point $x^- = k$ on a slice $\Sigma_-(x^+ = n)$ as u^n_k. The data u^{n+1}_k is determined from both u^{n+1}_{k-1} and u^n_k as in Fig. 2. Suppose we have already all the data at u^{n+1}_{k-1} and u^n_k.

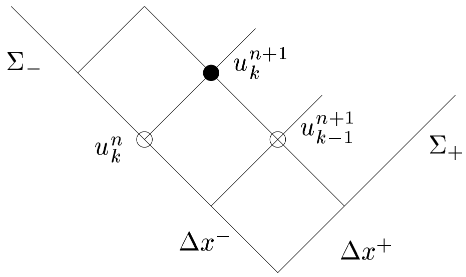

FIG. 2. The dual-null integration scheme. In order to obtain the data at grid u_k^{n+1}, we need both u_k^n and u_{k-1}^{n+1}.

(1) Firstly, we evolve along the x^+-direction, say from u_k^n to u_k^{n+1}. We have a set of equations for $(\Omega, f, \vartheta_\pm, \nu_-, k_{ab}, \varsigma_{-ab})$,

$$\Delta_+\Omega = -\tfrac{1}{2}\Omega^2\vartheta_+, \tag{3.16}$$
$$\Delta_+ f = \nu_+, \tag{3.17}$$
$$\Delta_+\vartheta_+ = -\nu_+\vartheta_+, \tag{3.18}$$
$$\Delta_+\vartheta_- = -\Omega(\tfrac{1}{2}\vartheta_+\vartheta_- + e^{-f}), \tag{3.19}$$
$$\Delta_+\nu_- = -\Omega^2(\tfrac{1}{2}\vartheta_+\vartheta_- + e^{-f}), \tag{3.20}$$
$$\Delta_+ k_{ab} = \Omega\varsigma_{+ab}, \tag{3.21}$$
$$\Delta_+\varsigma_{-ab} = \Omega(\varsigma_{+ac}k^{cd}\varsigma_{-db} - \tfrac{1}{2}\vartheta_-\varsigma_{+ab}). \tag{3.22}$$

The step is integrated using the Fehlberg method. Note that we do not have equations for evolving ν_+ and ς_+, therefore we have to interpolate them using $(\nu_+, \varsigma_{+ab})_k^n$ and $(\nu_+, \varsigma_{+ab})_k^{n+1}$. The latter was linearly extrapolated for the first iteration, but will be updated after an integration along the x^--direction (next step) has been done.

(2) Secondly, we evolve along the x^--direction, from u_{k-1}^{n+1} to u_k^{n+1}. We have a set of equations for (ν_+, ς_{+ab}),

$$\Delta_-\nu_+ = -\Omega^2(\tfrac{1}{2}\vartheta_+\vartheta_- + e^{-f}), \tag{3.23}$$
$$\Delta_-\varsigma_{+ab} = \Omega(\varsigma_{+ac}k^{cd}\varsigma_{-db} - \tfrac{1}{2}\vartheta_+\varsigma_{-ab}), \tag{3.24}$$

for completing the set u, but we also evolve $\vartheta_\pm, \Omega$ and f by

$$\Delta_-\Omega = -\tfrac{1}{2}\Omega^2\vartheta_- \tag{3.25}$$
$$\Delta_- f = \nu_-, \tag{3.26}$$
$$\Delta_-\vartheta_- = -\nu_-\vartheta_-, \tag{3.27}$$
$$\Delta_-\vartheta_+ = -\Omega(\tfrac{1}{2}\vartheta_+\vartheta_- + e^{-f}), \tag{3.28}$$

Here again we have to interpolate ς_- and ν_- in integrating the above, and we use a cubic spline interpolation using $(\nu_-, \varsigma_{-ab})_{k_i}^{n+1}$ $(1 \le k_i \le k)$, where the data $(\nu_-, \varsigma_{-ab})_k^{n+1}$ was given in the previous step (1).

(3) We check the consistencies of the evolution, by monitoring the differences of $(k_{ab}, \vartheta_\pm, \Omega, f)_k^n$ from the above step (1) and (2). If they are all within a tolerance, then we finish this evolution step by updating $(\nu_+, \varsigma_{+ab}, \vartheta_\pm, \Omega, f)$ as a value at u_k^{n+1}. If not, we repeat back to the step (1).

We construct a numerical grid in $x^\pm$ space with constant spacing in each direction. The iteration procedures are completed a couple of times at each grid point. The results shown in this article are obtained by setting the tolerance in the above step (3) to 10^{-5}. The code was tested for the Schwarzschild case, for which the analytic expression in dual-null coordinates is known; the calculated expansion $\vartheta_\pm$ differed from the exact expression to within 10^{-6}.

In the next section, we present our evolutions of a Kerr black-hole space-time under this quasi-spherical approximation. We chose the initial null slice Σ_- so as to cover the region $1.25r_H < r < r_0$. We stopped the evolution at $x^+ = 30$, which corresponds to r being $25 \sim 30m$, depending on the values of r_0 and a. We took 51 grid points in the x^- direction and 11 grid points in $\theta = [0, \pi/2]$, and evolved with grid separation $\Delta x^+ = 0.5\Delta x^-$.

IV. NUMERICAL RESULTS

Recall that our principal measures of the gravitational radiation are the conformal strain ε (2.27) and the specific energy E/m (2.30). Since we are using conformal variables, we expect that we can evolve towards the asymptotically flat region without long-term evolution in the x^+ direction. In Fig.3, we plotted the specific energy E/m at the boundaries of the integration region. We integrated the $\Delta_+ E$ equation of (2.30) along the hypersurface Σ_+ $(x^- = 0)$, setting $E = 0$ on S $(x^+ = x^- = 0)$, then integrated E using the $\Delta_- E$ equation at each constant x^+. We plotted E as a function of x^- at a constant x^+ surface in Fig.3(a). We see that E is converging to a line (the solid line in the figure), and not diverging even close to the black hole (at larger x^-). Fig.3(b) plots E at the final value of x^- as a function of x^+. We see from the figure that the energy measured for increasing x^+ converges at some value, as expected.

For the same set of parameters, we also plot the evolution behaviour of the conformal strain in Fig.4 and Fig.5. The cross component, $\varepsilon_\times = \varepsilon_{\theta\phi}$, is zero in this model, so only the plus component $\varepsilon_+ = \varepsilon_{\theta\theta}$ is needed. The conformal strain is calculated from (2.27) as a function of x^- at constant x^+ by setting $\varepsilon_+ = 0$ at $x^- = 0$. We again observe that ε_+ converges to particular lines (the solid lines) as x^+ increases, again reflecting the conformal variables. The line of $x^+ = 30.0$ in Fig.4, therefore, is close to the waveform for observers infinitely far from the source.

Note that the horizontal axis in Fig.4 is x^- coordinate, and this is related to $\Delta x^- \approx \sqrt{2}\Delta t$ at large distance, cf.

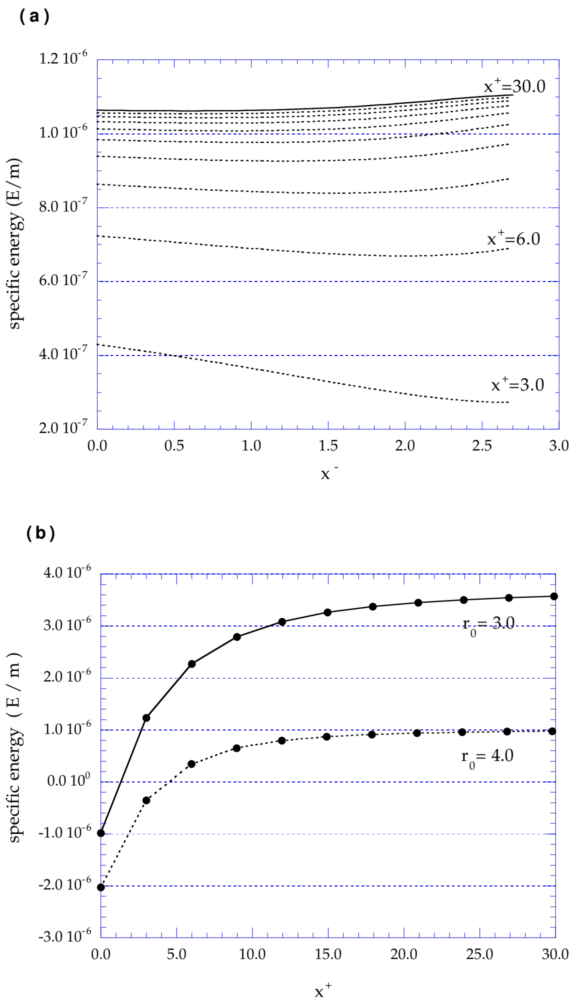

FIG. 3. Specific energy E/m for $a/m = 0.1$. (a) E/m is plotted as a function of the ingoing null coordinate x^- for each constant outgoing null coordinate $x^+ = 0.0, 3.0, \cdots, 30.0$. We set $r_0 = 4.0$ for this plot. (b) The integrated E/m over the ingoing null coordinate x^- is shown as a function of the outgoing null coordinate x^+. We show both $r_0 = 3.0$ and 4.0 cases. We see that the specific energy converges to a particular positive value in the x^+ direction, as expected.

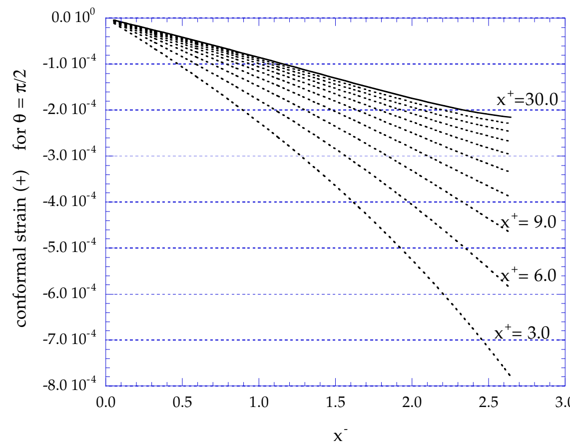

FIG. 4. Conformal strain ε_+ for $a/m = 0.1$ and $r_0 = 4.0$. The plot is for the equatorial plane $\theta = \pi/2$, showing the convergence of these lines in the x^+ direction. Lines are of $x^+ = 3.0, 6.0, 9.0, \cdots$, and 30.0. We remark that these lines are not wave-like.

(3.15). Then the unit length Δx^- for observers at large distance is about 5 $(m/M_\odot)\mu$ sec, translated from our units $c = G = 1$. Our plots in this article, therefore, covers a quite short time period compared with the typical millisecond timescale of gravitational waves from a Kerr black hole.* To obtain longer timescales we would have to integrate closer to the horizon, which causes numerical difficulties due to the infinite redshift. (This difficulty can be overcome using more computational resources, but becomes rather expensive.) However, for a dynamically evolving black hole, the event horizon has finite redshift and so could lie in the numerical integration region, allowing evolution to late times.

The magnitude of the conformal strain in Fig.4 is rescaled to the observable strain by (2.28). We can compare with an example of expected strain $\epsilon \sim 10^{-20}$ [9] for $R = 100$ Mpc by converting our units: $\epsilon = 3 \times 10^{-27}\varepsilon/(R/100 \text{ Mpc})$. This is small enough to validate the quasi-spherical approximation. The converged conformal strain ($x^+ = 30$ lines in Fig.4) is increasing as the ingoing coordinate x^- approaches the black hole horizon. However, if we extrapolate this magnitude to the horizon (which will be reached around $x^- \sim 6.0$ for this choice of parameter), it is still many orders of magnitude less than expected values.

Since Kerr spacetime is stationary, and its deviation from Schwarzschild spacetime is also stationary, a quasi-spherical approximation should produce time-independent errors, compounding over time to produce monotonic errors in the observable strain. This feature can be seen in the figures: the strain does not behave like a wave. (This fact is also confirmed for more wide range-covered calculation, up to 10 times longer in x^- range.) This result is good news for future applications of the quasi-spherical approximation, because the produced spurious waveform is quite different from a normal gravitational wave. We also show θ and a dependencies of ε_+ in Fig.5.

Our final, most conservative check of the quasi-spherical approximation is to compare the specific energy E/m with the expected specific energy of gravitational waves from an inspiralling black-hole binary. The Kerr black-hole space-time seems to be a good example for

---

*According to the quasi-normal mode analysis of the Kerr black hole [18], the dominant frequencies (fundamental mode corresponding to $l = 2$) of quasi-normal mode for a 10 $M_\odot$ black hole is between 1.2 kHz (for $a = 0$) and 1.8 kHz (for close to maximally rotating).

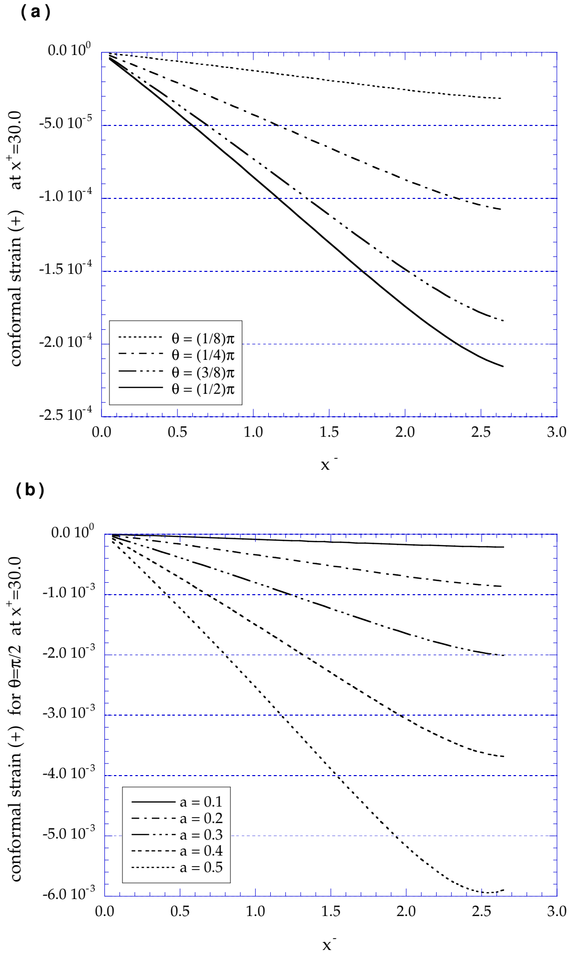

FIG. 5. Conformal strain ε_+ for the same parameters as Fig.4. (a) is ε_+ at $x^+ = 30.0$ for different θ. We see that the maximal strain occurs in the equatorial plane, $\theta = \pi/2$, as expected. (b) shows the dependence of ε_+ on a/m. The lines are for the data at $x^+ = 30.0$ for $\theta = \pi/2$. Both solid lines are equivalent with the solid line in Fig.4.

comparing with the result of the close-limit approach [9]. In Fig.6, we plotted the specific energy E/m due to spurious radiation, as a function of a/m and r_0/m. We applied the same grid points and other parameters in numerics with previous figures, and evaluated E/m at $x^+ = 30$. For higher a and larger r_0 cases, we could not fill plots in Fig.6. This is because we kept the resolutions and the same tolerance for the consistency convergence criteria for all cases, and these criteria failed for higher a and larger r_0. If we increase the resolutions and/or adjust the convergence criteria, then we can fill in these missing points also.

Consequently, we observe that the specific energy E/m increases with a/m and decreases with r_0/m, as expected. If we compare the amplitude of E/m with Fig.1 of Khanna *et al.* [9], then we find that our values are at least an order of magnitude smaller than the results of the close-limit approximation, up to the range where different versions of the latter diverge. The fact that the spurious radiation produced in the quasi-spherical approximation is quite small indicates the robustness of this approximation to the general situations.

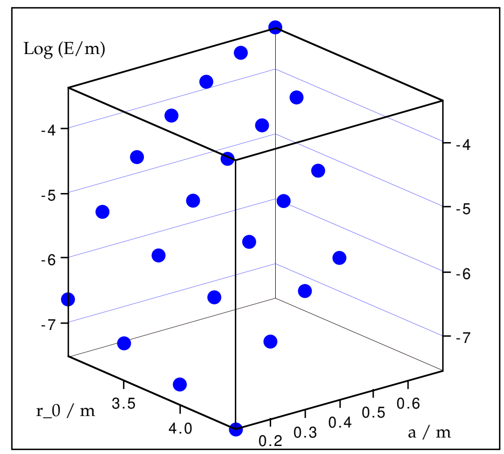

FIG. 6. Logarithmic plot of specific energy E/m due to spurious radiation, as a function of a/m and r_0/m. Energy is measured at $x^+ = 30$, and the plotted range is $r_0/m \in [3.0, 4.5]$ and $a/m \in [0.1, 0.7]$.

V. CONCLUDING REMARKS

We tested the quasi-spherical approximation by applying it to Kerr black holes. We numerically calculated the strain and energy flux of the spurious gravitational radiation produced from this approximation, and showed that (a) it converges quickly due to our conformal variables, (b) it does not behave like wave-like oscillations, and (c) the total radiated energy is at least an order of magnitude less than the gravitational radiation emission estimated from coalescing binary black holes, according to the close-limit approximation [9]. We remark that the close-limit approximation is the only current result which predicts the total amount of radiation from inspiralling binary black holes. Numerical results for head-on collisions with appreciable relative momentum also give similar estimates [8].

These results suggest that the spurious radiation does not fatally affect the gravitational waveform estimation. It might not affect the waveform estimation at all, and we might extract its effect to the total energy by subtracting the amount we showed in Fig.6. These facts directly encourage the robustness of the quasi-spherical approximation. Therefore we are interested in applying this scheme to more general situations, and/or implementing it as an output routine for full numerical simulation codes of binary black holes or compact stars, such as those using the standard 3+1 decomposition of spacetime. These efforts will be reported elsewhere.

Recently, one of the authors extended the quasi-spherical approximation to include non-linear terms in the shears [19]. We have also tested this second approximation numerically using the same model and method. We find that the difference between the two levels of approximation is numerically indistinguishable, e.g. the specific energy shown in Fig.6 is identical to three digits. Thus the application also passes the reliability test provided by a comparision of first and second approximations.

ACKNOWLEDGMENTS

We thank communications with Abhay Ashtekar, Pablo Laguna, Luis Lehner, Shinji Mukohyama, Jorge Pullin and John Stewart. We appreciate the hospitality of the CGPG group. HS was supported by the Japan Society for the Promotion of Science as a research fellow abroad. SAH was supported by the National Science Foundation under award PHY-9800973.

[1] S.A. Hayward, Phys. Rev. **D61**, 101503 (2000).
[2] N. T. Bishop, R. Gómez, L Lehner, and J. Winicour, Phys. Rev. **D54**, 6153 (1996).
[3] N.T. Bishop, R. Gómez, L. Lehner, M. Maharaj, and J. Winicour, Phys. Rev. **D56**, 6298 (1997).
Binary Black Hole Grand Challenge Alliance, Phys. Rev. Lett. **80**, 3915 (1998).
See also a recent review by J. Winicour, Prog. Theor. Phys. Suppl. **136**, 57 (1999).
[4] *e.g.,* Y. Mino, M. Sasaki, M. Shibata, H. Tagoshi and T. Tanaka, Prog. Theor. Phys. Suppl. **128** (1997) 1.
[5] *e.g.,* S.R. Brandt and E. Seidel, Phys. Rev. **D52** (1995) 856; Phys. Rev. **D52** (1995) 870; Phys. Rev. **D54** (1996) 1403
[6] P. Anninos, D. Hobill, E. Seidel, L. Smarr, and W-M. Suen, Phys. Rev. Lett. **71**, 2851 (1993); Phys. Rev. **D52**, 2044 (1995).
[7] P. Anninos, R.H. Price, J. Pullin, E. Seidel, and W-M. Suen, Phys. Rev. **D52**, 4462 (1995).
[8] J. Baker, A. Abrahams, P. Anninos, S. Brandt, R. Price, J. Pullin, and E. Seidel, Phys. Rev. **D55**, 829 (1997).
[9] G. Khanna, J. Baker, R. J. Gleiser, P. Laguna, C.O. Nicasio, H-P. Nollert, R. Price and J. Pullin, Phys. Rev. Lett. **83**, 3581 (1999).
See also a recent review by J. Pullin, Prog. Theor. Phys. Suppl. **136**, 107 (1999).
[10] D. Christodoulou, Phys. Rev. Lett. **25**, 1596 (1970). R. M. Wald, *General Relativity* (Chicago Univ. Press, 1984).
[11] S.A. Hayward, Ann. Inst. H. Poincaré **59**, 399 (1993).
[12] S.A. Hayward, Class. Quantum Grav. **10**, 779 (1993).
[13] B. Carter, Phys. Rev. **141**, 1242 (1966). [see e.g. S. Chandrasekhar, *The Mathematical Theory of Black Holes* (Oxford Univ. Press, 1992).]
[14] F. Pretorius and W. Israel, Class. Quantum Grav. **15**, 2289 (1998).
[15] We thank Shinji Mukohyama for discussing this part.
[16] C. Gundlach and J. Pullin, Class. Quantum Grav. **14**, 991 (1997).
[17] R. S. Hamadé and J. M. Stewart, Class. Quantum Grav. **13**, 497 (1996).
[18] E.W. Leaver, Proc. R. Soc. Lond. **A402** (1985) 285.
[19] S.A. Hayward, Gravitational-wave energy and radiation reaction on quasi-spherical black holes, gr-qc/0012077.
S.A. Hayward, Gravitational-wave and black-hole dynamics: second quasi-spherical approximation, gr-qc/0102013.